

MegaFusion: Extend Diffusion Models towards Higher-resolution Image Generation without Further Tuning

Haoning Wu^{1,2*}, Shaocheng Shen^{1,3*}, Qiang Hu¹, Xiaoyun Zhang¹, Ya Zhang^{1,2}, Yanfeng Wang^{1,2}

¹Shanghai Jiao Tong University, China ²Shanghai AI Laboratory, China

³Dalian University of Technology, China



Figure 1. **Overview.** *Left:* Existing diffusion-based text-to-image models fall short in synthesizing higher-resolution images due to the fixed image resolution during training, resulting in a noticeable decline in image quality and semantic deviation. *Right:* Our proposed tuning-free **MegaFusion** can effectively and efficiently extend diffusion models (e.g. SDM [35], SDXL [30] and Floyd [6]) towards generating images at higher resolutions (e.g., 1024×1024 , 1920×1080 , 2048×1536 , and 2048×2048) of arbitrary aspect ratios (e.g., $1 : 1$, $16 : 9$, and $4 : 3$). We recommend the reader to zoom in for the visualization results.

Abstract

Diffusion models have emerged as frontrunners in text-to-image generation for their impressive capabilities. Nonetheless, their fixed image resolution during training often leads to challenges in high-resolution image generation, such as semantic inaccuracies and object replication. This paper introduces **MegaFusion**, a novel approach that extends existing diffusion-based text-to-image generation models towards efficient higher-resolution generation without additional fine-tuning or extra adaptation. Specifically, we employ an innovative **truncate and relay** strategy to bridge the denoising processes across different resolutions, allowing for high-resolution image generation in a coarse-to-fine manner. Moreover, by integrating dilated

convolutions and noise re-scheduling, we further adapt the model's priors for higher resolution. The versatility and efficacy of **MegaFusion** make it universally applicable to both latent-space and pixel-space diffusion models, along with other derivative models. Extensive experiments confirm that **MegaFusion** significantly boosts the capability of existing models to produce images of megapixels and various aspect ratios, while only requiring about 40% of the original computational cost. Code is available at <https://haoningwu3639.github.io/MegaFusion/>.

1. Introduction

Diffusion models have recently demonstrated unparalleled performance across broad applications, including text-to-image generation [6, 14–16, 35, 40], image editing [3, 12, 21, 26, 28, 45], consistent image sequence generation [25, 27, 29], and even achieves promising results in

*: These authors contribute equally to this work.

challenging text-to-video generation [14, 17, 39, 46]. Among them, the open-source Stable Diffusion (also known as Latent Diffusion [35]) leverages a pre-trained VAE [22] to compress images into a latent space for efficiency. After pre-training on large-scale paired datasets like LAION-5B [38], it has showcased impressive generative capabilities, thus being widely employed. In comparison, Imagen [37] and Floyd [6] opt for a cascading diffusion model in pixel space, initiating with low-resolution image synthesis followed by successive super-resolution stages to enable high-resolution text-to-image generation.

Despite these advancements, as depicted in Figure 1 *Left*, these models face a significant hurdle: they struggle to generate images beyond the training range’s resolution, leading to semantic deviation and a decline in image quality. Existing efforts to address these issues often require extra tuning or are limited to specific models. For example, MultiDiffusion [2] and ElasticDiffusion [10] adopt post-processing or optimization techniques to stitch native-resolution images into higher-resolution panoramas, which is inefficient and time-consuming. Relay Diffusion [41] employs blurring diffusion and block noise in pixel space, yet it necessitates training multiple specific diffusion models from scratch. ResAdapter [5] and CheapScaling [9] introduce minimal extra training through LoRA [19] layers or Up-samplers, but still incur a non-negligible training overhead. Meanwhile, tuning-free alternatives like ScaleCrafter [11] and FouriScale [20] adapt pre-trained SDMs for higher resolution synthesis, but require meticulous hyperparameter adjustment and are restricted to latent-space models.

To tackle the aforementioned limitations, we introduce **MegaFusion**, a powerful tuning-free method to extend existing diffusion models towards generating higher-resolution and variable aspect ratio images with megapixels. Concretely, we begin with a *truncate and relay* strategy, which seamlessly bridges the synthesis of different resolution images, enabling efficient higher-resolution generation in a coarse-to-fine manner with only about 40% of the original computational cost. Additionally, we further improve the quality and details of generated images through *dilated convolutions* [49] and *noise re-scheduling*. The versatility and effectiveness of our **MegaFusion** make it compatible with both latent-space and pixel-space diffusion models, and its foundational principles can be extended to other diffusion-based frameworks with extra conditions, such as IP-Adapter [48] and ControlNet [51]. As shown in Figure 1 *Right*, MegaFusion significantly improves the ability of diffusion models to synthesize higher-resolution images that are both semantically accurate and of superior quality.

To summarize, we make the following contributions in this paper: (i) we propose a tuning-free approach, **MegaFusion**, that utilizes a *truncate and relay* strategy to efficiently generate high-quality, high-resolution images with

megapixels in a coarse-to-fine manner; (ii) we incorporate *dilated convolution* and *noise re-scheduling* techniques to further refine the adaptability of pre-trained diffusion models for higher resolution; (iii) we demonstrate the applicability of our method across both latent-space and pixel-space diffusion models, as well as their extensions, enabling the generation of high-resolution images with various aspect ratios at roughly 40% of the original computational expense; (iv) we conduct extensive experiments to validate the effectiveness and superiority of our proposed method, in terms of efficiency, image quality, and semantic accuracy.

2. Related Works

Diffusion Models. As a groundbreaking family in probabilistic generative models, diffusion models progressively inject noise into data in a forward process and learn to invert this process to generate new samples. DDPM [15] has showcased remarkable performance, outperforming previous GAN-based and auto-regressive techniques, while DDIM [40] significantly improves sampling efficiency. Leveraging their excellent generative capabilities, diffusion models have been applied to diverse fields, including image-to-image translation [3, 12, 21, 26, 28, 45], image sequence generation [25, 27, 29] and video generation [14, 17, 39, 46].

Text-to-Image Generation. Generative models have been widely adopted for the challenging text-to-image generation task, with GAN [8] and its variants [47, 50] as the pioneers. Meanwhile, auto-regressive transformers like DALL-E [34] further push the boundaries. Recently, diffusion models, such as DALL-E 2 [33], Imagen [37] and Floyd [6], have risen to prominence in text-to-image generation tasks. Notably, Stable Diffusion (Latent Diffusion Models [35]), performing the diffusion process in latent space, has demonstrated outstanding performance after extensive pre-training on vast image-text pair datasets, thereby being widely applied within the research community. Additionally, SDXL [30] further elevates the generative performance with a diffusion refiner and an extra text encoder.

Our **MegaFusion**, is designed for seamless integration with diffusion models across both latent and pixel spaces, extending their capacity for higher-resolution generation.

Higher-resolution Generation. Although diffusion models have shown promising performance in image generation, they are typically limited to fixed resolutions and aspect ratios, struggling to synthesize higher-resolution images beyond their training data. MultiDiffusion [2] addresses this by synthesizing overlapping crops with a pre-trained diffusion model and merging these to produce panoramic images, but it requires a time-consuming inference procedure. ElasticDiffusion [10] adopts a similar approach and improves image quality via reference images and reduced-resolution guidance. Relay Diffusion [41] constructs a

pixel-space diffusion model with blurring diffusion and block noise to craft high-resolution images, at the cost of re-training several models from scratch. ScaleCrafter [11] improves high-resolution generation by addressing the UNet’s insufficient receptive field with dispersed convolution, without additional fine-tuning on Stable Diffusion. DemoFusion [7] attempts to connect multiple resolutions for coarse-to-fine generation, but it requires repeating multiple image generation processes, leading to low inference efficiency.

Several concurrent works also express rich interest in higher-resolution generation: ResAdapter [5] introduces a trainable adapter to generate images with unrestricted resolutions and aspect ratios by understanding resolution priors. CheapScaling [9] integrates multi-scale upsampler modules for multi-resolution generation with minimal tuning. FouriScale [20] and HiDiffusion [52] offer a training-free strategy but are still limited to SDM-based models.

In contrast to the aforementioned methods, which either necessitate further training or are limited to specific models, our proposed **MegaFusion** emerges as a versatile solution. It can be seamlessly integrated into both latent-space and pixel-space diffusion models, without any extra tuning or adaptation, synthesizing higher-resolution images of various aspect ratios with megapixels.

3. Preliminary

In this section, we briefly introduce diffusion models, including their forward and backward processes in Sec. 3.1; and the latent diffusion models (LDMs) that perform diffusion in latent space to improve efficiency in Sec. 3.2.

3.1. Diffusion Models

Diffusion models, a type of deep generative models, fundamentally transform input Gaussian noise into structured data samples through iterative denoising. Concretely, diffusion models comprise a forward diffusion process that progressively adds Gaussian noise to an image \mathbf{x}_0 via a Markov process over T steps. Let \mathbf{x}_t represent the noisy image at step t , with the transition from \mathbf{x}_{t-1} to \mathbf{x}_t being modeled by $q(\mathbf{x}_t|\mathbf{x}_{t-1}) = \mathcal{N}(\mathbf{x}_t; \sqrt{1 - \beta_t} \mathbf{x}_{t-1}, \beta_t \mathbf{I})$. Here, $\beta_t \in (0, 1)$ are pre-determined hyperparameters controlling the variance introduced at each step.

Defining $\alpha_t = 1 - \beta_t$ and $\bar{\alpha}_t = \prod_{i=1}^t \alpha_i$, we can leverage the properties of Gaussian distributions and the reparameterization trick to reformulate the relationship as: $q(\mathbf{x}_t|\mathbf{x}_0) = \mathcal{N}(\mathbf{x}_t; \sqrt{\bar{\alpha}_t} \mathbf{x}_0, (1 - \bar{\alpha}_t) \mathbf{I})$. This insight allows us to succinctly express the forward process with Gaussian noise ϵ as: $\mathbf{x}_t = \sqrt{\bar{\alpha}_t} \mathbf{x}_0 + \sqrt{1 - \bar{\alpha}_t} \epsilon$.

Diffusion models also encompass a reverse diffusion process to reconstruct an image from noise. This process, denoted as p_θ , usually leverages a UNet-based [36] model to estimate the noise term ϵ_θ , represented as: $p_\theta(\mathbf{x}_{t-1}|\mathbf{x}_t) = \mathcal{N}(\mathbf{x}_{t-1}; \mu_\theta(\mathbf{x}_t, t), \Sigma_\theta(\mathbf{x}_t, t))$.

Here, μ_θ represents the predicted mean value of Gaussian distribution, which can be expressed in terms of the noise ϵ_θ as: $\mu_\theta(\mathbf{x}_t, t) = \frac{1}{\sqrt{\alpha_t}} (\mathbf{x}_t - \frac{1 - \alpha_t}{\sqrt{1 - \bar{\alpha}_t}} \epsilon_\theta(\mathbf{x}_t, t))$

3.2. Latent Diffusion Models

To improve efficiency and reduce computational cost, Latent Diffusion (LDMs) execute diffusion and denoising within a learned low-dimensional latent space of a pre-trained Variational Autoencoder (VAE). Specifically, the VAE encoder \mathcal{E} converts an image $\mathbf{x}_0 \in \mathbb{R}^{3 \times H \times W}$ into a latent representation $\mathbf{z}_0 \in \mathbb{R}^{4 \times h \times w}$ via $\mathbf{z}_0 = \mathcal{E}(\mathbf{x}_0)$. Afterwards, the decoder \mathcal{D} reconstructs the original image \mathbf{x}_0 from \mathbf{z}_0 , represented as $\hat{\mathbf{x}}_0 = \mathcal{D}(\mathbf{z}_0) \approx \mathbf{x}_0$.

This setup allows the diffusion process to be conducted in a compact latent space, enabling efficient image synthesis. During inference, LDM samples latent codes from a conditional distribution $p(\mathbf{z}_0|c)$, where c represents the conditional information such as text embedding from CLIP [31] or T5 [32] text encoder. This process can be formalized as: $p_\theta(\mathbf{z}_{t-1}|\mathbf{z}_t, c) = \mathcal{N}(\mathbf{z}_t; \mu_\theta(\mathbf{z}_t, t, c), \Sigma_\theta(\mathbf{z}_t, t, c))$

4. Method

This section initiates with elaborating on the *truncate and relay* strategy within our proposed tuning-free **MegaFusion** in Sec. 4.1. Then, we incorporate *dilated convolution* and *noise re-scheduling* to further adapt model prior towards higher resolution in Sec. 4.2. Lastly, we detail the application of our method across latent-space and pixel-space diffusion models, as well as their extensions, in Sec. 4.3.

4.1. Truncate and Relay Strategy

For clarity, we will explain our method using latent-space diffusion models as an example. As for diffusion models in pixel space, our method can be applied more straightforwardly and conveniently.

With a pre-trained Stable Diffusion Model (SDM) equipped with a denoiser ϵ_θ , a low-resolution latent code $\mathbf{z}_0^1 \in \mathbb{R}^{4 \times h_1 \times w_1}$ can be synthesized within T denoising steps, then decoded into an image $\mathbf{x}_0^1 \in \mathbb{R}^{3 \times H_1 \times W_1}$ by the VAE decoder \mathcal{D} . Conditioned on a text prompt c_T , our goal is to generate a higher-resolution image $\mathbf{x}_0^k \in \mathbb{R}^{3 \times H_k \times W_k}$ alongside its corresponding latent code $\mathbf{z}_0^k \in \mathbb{R}^{4 \times h_k \times w_k}$, by linking the generation processes across different resolutions over a total of T steps, where $T = \sum_{i=1}^k T_i$.

Given that our methodology is inherently tuning-free, we focus on the inference stage herein. We begin with a low-resolution generation through T_1 steps denoising:

$$\mathbf{z}_t = \frac{1}{\sqrt{\alpha_t}} (\mathbf{z}_t - \frac{1 - \alpha_t}{\sqrt{1 - \bar{\alpha}_t}} \epsilon_\theta(\mathbf{z}_t, t, c_T)) + \sigma_t \epsilon, \quad (1)$$

where $t = T, T - 1, \dots, T - T_1 + 1$

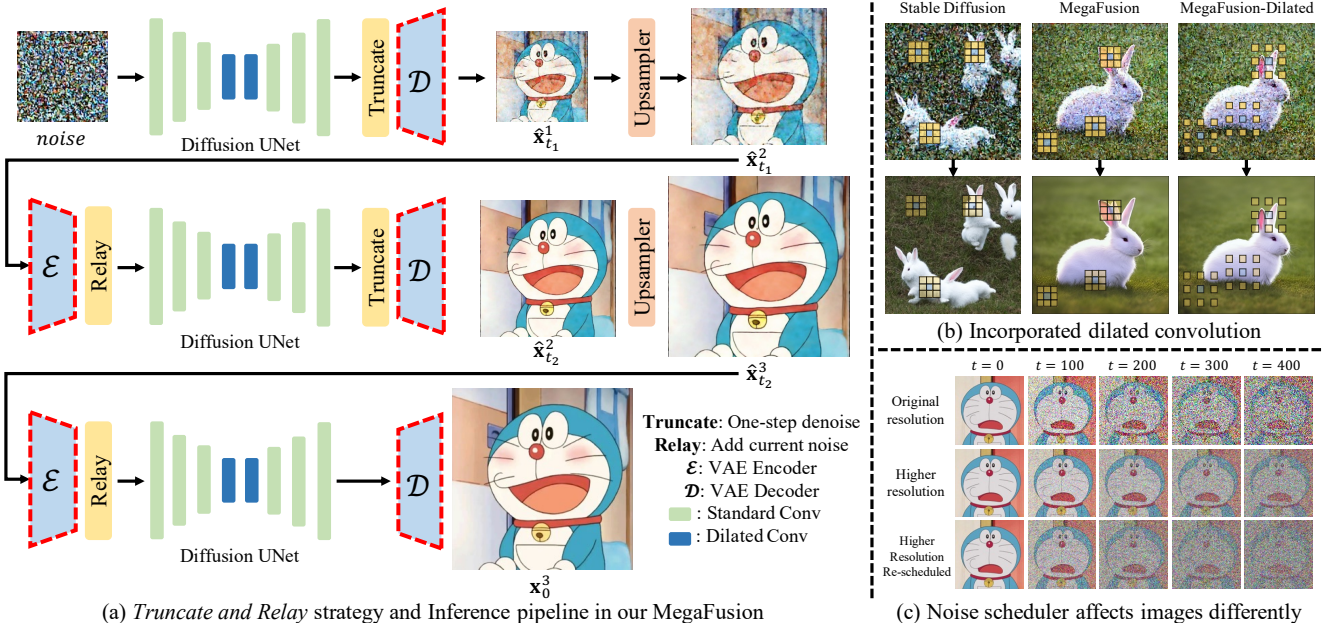


Figure 2. **Architecture Overview.** (a) The *Truncate and Relay* strategy in **MegaFusion** seamlessly connects generation processes across different resolutions to produce higher-resolution images without extra tuning, exemplified by a three-stage pipeline. For pixel-space models, the VAE encoder and decoder can be directly removed. (b) Limited receptive fields lead to quality decline and object replication. *Dilated convolutions* expand the receptive field at higher resolutions, enabling the model to capture more global information for more accurate semantics and image details. (c) Noise at identical timesteps affects images of different resolutions differently, deviating from the model’s prior. *Noise re-scheduling* helps align the noise level of higher-resolution images with that of the original resolution.

where σ_t are pre-calculated coefficients and ϵ denotes noise sampled from a standard Gaussian distribution. Subsequently, at step $t_1 = T - T_1 + 1$, we **truncate** the generation process and compute the approximate clean latent code $\hat{\mathbf{z}}_{t_1}^1 \in \mathbb{R}^{4 \times h_1 \times w_1}$, which serves as a pivotal element for multi-resolutions bridging:

$$\hat{\mathbf{z}}_{t_1}^1 = \frac{1}{\sqrt{\bar{\alpha}_{t_1}}} (\mathbf{z}_{t_1} - \sqrt{1 - \bar{\alpha}_{t_1}} \epsilon_{\theta}(\mathbf{z}_{t_1}, t_1, c_T)) \quad (2)$$

Here, $\hat{\mathbf{z}}_{t_1}^1$ is subsequently decoded to an image $\hat{\mathbf{x}}_{t_1}^1 \in \mathbb{R}^{3 \times H_1 \times W_1}$ and upsampled to a higher-resolution relatively clean image $\hat{\mathbf{x}}_{t_1}^2 \in \mathbb{R}^{3 \times H_2 \times W_2}$ utilizing a non-parametric Upsampler, Φ , represented as:

$$\hat{\mathbf{x}}_{t_1}^1 = \mathcal{D}(\hat{\mathbf{z}}_{t_1}^1), \quad \hat{\mathbf{x}}_{t_1}^2 = \Phi(\hat{\mathbf{x}}_{t_1}^1) \quad (3)$$

Then, the upsampled image $\hat{\mathbf{x}}_{t_1}^2$ is re-encoded into to latent code $\hat{\mathbf{z}}_{t_1}^2 \in \mathbb{R}^{4 \times h_2 \times w_2}$ via the VAE encoder \mathcal{E} and perturbed with noise at the current step t_1 to **relay** the generation:

$$\hat{\mathbf{z}}_{t_1}^2 = \mathcal{E}(\hat{\mathbf{x}}_{t_1}^2), \quad \mathbf{z}_{t_1}^2 = \mathcal{N}(\mathbf{z}_{t_1}^2; \sqrt{\bar{\alpha}_{t_1}} \hat{\mathbf{z}}_{t_1}^2, (1 - \bar{\alpha}_{t_1}) \mathbf{I}) \quad (4)$$

The generation process continues at a higher resolution, by re-leveraging Equation 1 for T_2 steps of denoising, sequentially navigating through $t = T - T_1, T - T_1 - 1, \dots, T - T_1 - T_2 + 1$. Subsequently, the *truncate and relay* operations can be then conducted at step $t_2 = T - T_1 - T_2 + 1$.

As depicted in Figure 2 (a), this iterative process is repeated multiple times until the generation of a high-resolution latent code \mathbf{z}_0^k , which can be then decoded into a corresponding high-resolution image \mathbf{x}_0^k with megapixels.

4.2. MegaFusion++

Our MegaFusion, based on the *truncate and relay* strategy, can be further combined orthogonally with existing techniques such as *dilated convolution* and *noise rescheduling*, to adapt the model priors to higher resolutions.

Dilated Convolution. Blurriness and semantic deviation in high-resolution images from diffusion models can be attributed to the constrained receptive field of UNet layers trained on fixed-resolution data, which lack comprehensive global information. For instance, as illustrated in Figure 2 (b), existing models trained on low-resolution images tend to synthesize multiple rabbits in different local areas due to insufficient receptive fields, leading to semantic inaccuracies. Inspired by ScaleCrafter [11], we modify the convolutional kernels of the UNet-based denoiser ϵ_{θ} to incorporate dilated convolutions [49] with a specific dilation rate δ . This broadens the model’s receptive field without additional tuning, allowing for better incorporation of global information.

For the sake of simplicity, we omit channel dimension and convolution biases here, focusing on the modification of weight parameters to transform standard convolutions into dilated counterparts. Given a feature map

Methods	resolution	$ FID_r \downarrow $	$ FID_b \downarrow $	$ KID_r \downarrow $	$ KID_b \downarrow $	$ CLIP-T \uparrow $	$ CIDEr \uparrow $	$ Metor \uparrow $	$ ROUGE \uparrow $	GFlops	Inference time
SDM [35]	1024×1024	41.35	51.02	0.0086	0.0113	0.3009	17.75	18.38	23.64	135.0K	15.17s
SDM-StableSR [44]	1024×1024	25.46	19.61	0.0062	0.0031	0.3117	20.24	20.91	26.28	292.6K	33.48s
ScaleCrafter [11]	1024×1024	27.97	22.05	0.0076	0.0043	0.3125	20.14	21.65	28.23	135.0K	17.52s
SDM-MegaFusion	1024×1024	30.19	10.98	0.0088	0.0034	0.3101	21.14	21.44	27.34	48.2K	7.56s
SDM-MegaFusion++	1024×1024	25.14	7.82	0.0064	0.0012	0.3121	20.46	22.18	28.36	48.2K	7.56s
SDXL [30]	2048×2048	47.53	47.08	0.0133	0.0139	0.3041	17.55	18.65	25.10	540.2K	79.66s
ScaleCrafter [11]	2048×2048	27.46	24.73	0.0064	0.0061	0.3138	19.97	22.34	28.12	540.2K	80.72s
DemoFusion [7]	2048×2048	24.61	13.36	0.0066	0.0023	0.3198	22.02	22.86	28.48	1354.9K	217.19s
SDXL-MegaFusion	2048×2048	25.12	12.13	0.0059	0.0027	0.3227	23.49	22.65	28.12	216.1K	30.94s
SDXL-MegaFusion++	2048×2048	23.86	6.93	0.0056	0.0018	0.3244	23.42	22.74	28.38	216.1K	30.94s
Floyd-Stage1 [6]	128×128	66.27	81.65	0.0262	0.0454	0.2818	14.69	18.22	25.06	111.7K	77.08s
Floyd-MegaFusion	128×128	53.09	39.73	0.0273	0.0334	0.3024	25.01	25.00	31.35	44.9K	32.19s
Floyd-MegaFusion++	128×128	43.43	50.08	0.0213	0.0437	0.3046	20.28	25.01	31.64	44.9K	32.19s
Floyd-Stage2 [6]	512×512	46.64	38.15	0.0254	0.0166	0.3098	23.85	21.47	26.26	60.7K	48.58s
Floyd-MegaFusion	512×512	39.80	24.87	0.0164	0.0078	0.3106	23.22	23.51	29.30	24.3K	21.72s
Floyd-MegaFusion++	512×512	26.34	24.55	0.0063	0.0077	0.3110	24.01	23.58	29.52	24.3K	21.72s

Table 1. **Quantitative comparison.** We compare our boosted models on higher-resolution image generation with representative latent-space and pixel-space diffusion models on the MS-COCO [24] dataset. Within each unit, we denote the best performance in **RED** and the second-best performance in **BLUE**.

$F \in \mathbb{R}^{m \times n}$ and a convolutional kernel $k \in \mathbb{R}^{r \times r}$, the standard convolution can be represented as: $(F * k)(p) = \sum_{s+t=p} F(s) \cdot k(t)$. In contrast, the corresponding dilated convolution, with dilation rate δ , can be expressed as: $(F *_{\delta} k)(p) = \sum_{s+\delta t=p} F(s) \cdot k(t)$. Here, p, k , and t denote spatial locations within the feature map and convolution kernel, respectively.

Rather than replacing all convolutions with dilated ones, which may lead to catastrophic quality decline, we selectively apply this modification to the middle layers of UNet. **The insight here is that:** we wish to broaden the receptive field in the bottleneck to aggregate global information, while simultaneously preserving original priors at higher resolution to sample nearby features for enhancing details.

Noise Re-scheduling. Similar to discoveries in simple diffusion [18] and relay diffusion [41], we observe that identical noise levels impact images differently across various resolutions, as depicted in Figure 2 (c), resulting in varying signal-to-noise ratios (SNR) at the same timestep.

According to the SNR definition in previous work [18]: $SNR_t = \frac{(\sqrt{\bar{\alpha}_t})^2}{(\sqrt{1-\bar{\alpha}_t})^2} = \frac{\bar{\alpha}_t}{1-\bar{\alpha}_t}$. Considering a low-resolution image $\mathbf{x} \in \mathbb{R}^{3 \times H \times W}$ and a high-resolution one $\mathbf{x}' \in \mathbb{R}^{3 \times H' \times W'}$ with $H' = 2H$ and $W' = 2W$, if we down-sample \mathbf{x}' to $\mathbf{x}'_{down} \in \mathbb{R}^{3 \times H \times W}$, the SNR at timestep t of \mathbf{x}'_{down} (denoted as $SNR_{down}^{H' \times W'}$) in comparison to \mathbf{x} (represented as $SNR^{H \times W}$) will exhibit the following relationship: $SNR^{H \times W} = \gamma \cdot SNR_{down}^{H' \times W'}$.

Assuming the original noise scheduler at $H \times W$ is denoted as $\bar{\alpha}_t$, the revised scheduler $\bar{\alpha}'_t$ at higher resolution $H' \times W'$ should satisfy: $\frac{\bar{\alpha}_t}{1-\bar{\alpha}_t} = \gamma \cdot \frac{\bar{\alpha}'_t}{1-\bar{\alpha}'_t}$. This yields the

relationship: $\bar{\alpha}'_t = \frac{\bar{\alpha}_t}{\gamma - (\gamma - 1)\bar{\alpha}_t}$. Incorporating this into the high-resolution noise scheduler initialization gives a new $\bar{\alpha}'_t$ sequence. This process, called noise re-scheduling, adjusts noise levels to better suit higher-resolution image generation, thereby improving synthesis quality and fidelity.

4.3. Further Application on other Models

Pixel-space Diffusion Models. Similar to latent-space models, our proposed MegaFusion is equally applicable to pixel-space diffusion models, e.g. Floyd [6]. The primary distinction lies in performing the *truncate and relay* operation directly in pixel space. This implies that Equations 2, 3 and 4 can be adapted as follows:

$$\hat{\mathbf{x}}_{t_1}^1 = \frac{1}{\sqrt{\bar{\alpha}_{t_1}}} (\mathbf{x}_{t_1} - \sqrt{1-\bar{\alpha}_{t_1}} \epsilon_{\theta}(\mathbf{x}_{t_1}, t_1, c_T)) \quad (5)$$

$$\hat{\mathbf{x}}_{t_1}^2 = \Phi(\hat{\mathbf{x}}_{t_1}^1), \quad \mathbf{x}_{t_1}^2 = \mathcal{N}(\mathbf{x}_{t_1}^2; \sqrt{\bar{\alpha}_{t_1}} \hat{\mathbf{x}}_{t_1}^2, (1-\bar{\alpha}_{t_1}) \mathbf{I}) \quad (6)$$

Diffusion Models with Extra Conditions. Beyond the scope of text-to-image foundation models, our methodology can extend to diffusion models that incorporate extra input conditions, such as ControlNet [51] and IP-Adapter [48]. These models use both text condition c_T and image condition c_I as input. Consequently, Equation 1 can be reformulated to accommodate both conditions:

$$\mathbf{z}_t = \frac{1}{\sqrt{\bar{\alpha}_t}} (\mathbf{z}_t - \frac{1-\bar{\alpha}_t}{\sqrt{1-\bar{\alpha}_t}} \epsilon(\mathbf{z}_t, t, c_T, c_I)) + \sigma_t \epsilon \quad (7)$$

5. Experiments

In this section, we start by outlining our experimental settings in Sec. 5.1. Subsequently, we present compar-

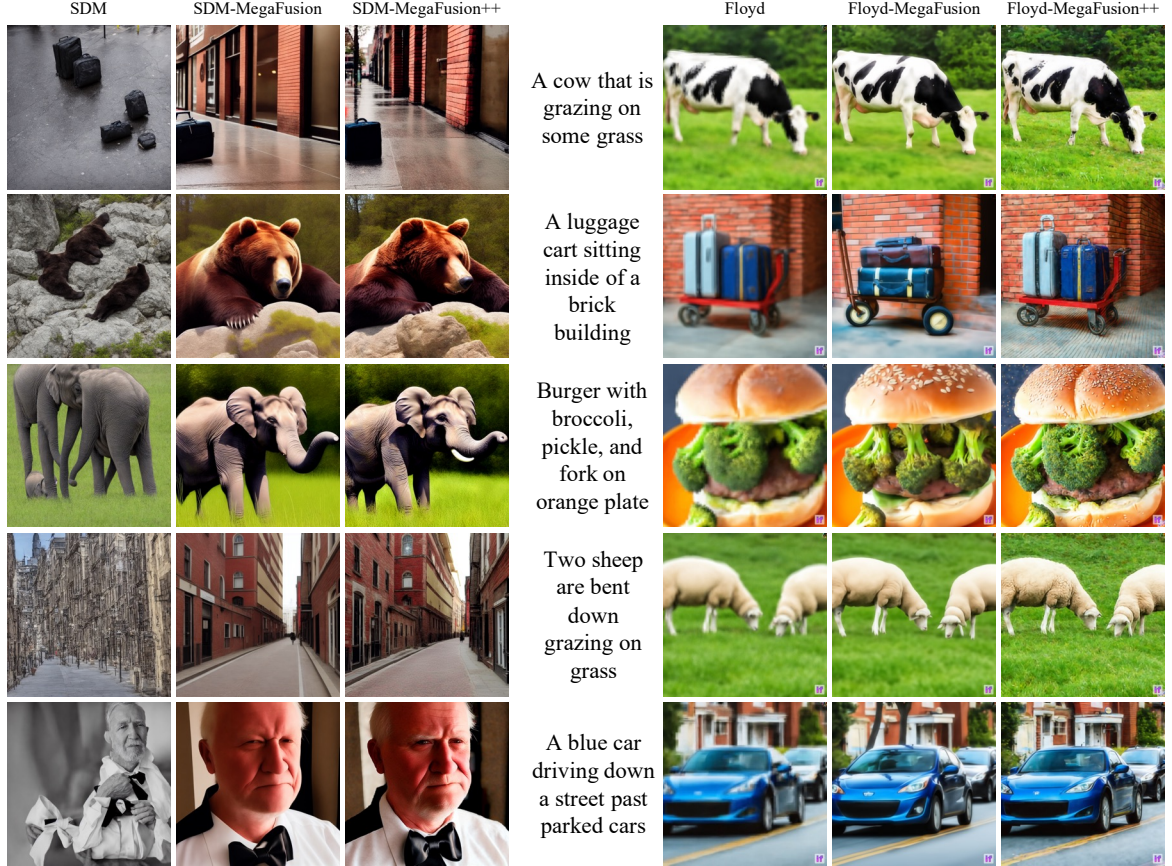


Figure 3. **Qualitative results** of applying our MegaFusion to both latent-space and pixel-space diffusion models for higher-resolution image generation on MS-COCO and commonly used prompts from the Internet. Our method can effectively extend existing diffusion-based models towards synthesizing higher-resolution images of megapixels with correct semantics and details.

isons to existing models with quantitative metrics and human evaluation in Sec. 5.2. We then showcase qualitative results of applying our method to various diffusion models in Sec. 5.3. Lastly, ablation studies are presented in Sec. 5.4 to validate the efficacy of our proposed components.

5.1. Experiment Settings

Implementation Details. We evaluate text-to-image diffusion models in both latent space (SDM 1.5 [35] and SDXL [30]) and pixel space (Floyd [6]). All models use DDIM [40] for $T = 50$ steps of sampling except in cases explicitly stated otherwise. Given that SDM is trained with a fixed resolution of 512×512 , we choose to generate high-resolution images of 1024×1024 for quantitative comparison. Specifically, we orchestrate generation across $k = 3$ resolutions: 512, 768 and 1024, with respective denoising steps of $T_1 = 40$, $T_2 = 5$, and $T_3 = 5$. Furthermore, our proposed MegaFusion can be applied to synthesize 2048×2048 and even higher-resolution images with SDM for qualitative assessment. SDXL defaults to synthesizing images of 1024×1024 , considering the balance of computational costs, we discard the Refiner module and

employ two-stage generation, 1024 and 2048, with their respective denoising steps being $T_1 = 40$ and $T_2 = 10$.

On the other hand, Floyd, a 3-stage cascaded model, sequentially upscales images from 64×64 to 256×256 , culminating in 1024×1024 images. Due to computational constraints, only the initial two stages of Floyd are employed in our experiments. The first stage necessitates 100 steps of DDIM sampling ($T_1 = 80$ for generating 64×64 images, and $T_2 = 20$ for 128×128), while the second stage requires 50 steps (40 for $T_1 = 256 \times 256$ and $T_2 = 10$ for 512×512).

Bicubic upsampling serves as the default non-parametric Upsampler Φ . For dilated convolutions, we set the dilation rate $\delta = 2$, and select the hyperparameter $\gamma = 4$ for noise re-scheduling. All experiments are conducted on a single Nvidia RTX A40 GPU, with SDM and SDXL in *float16* half-precision, and Floyd at *float32* full-precision.

Evaluation Datasets. We assess our method and baseline models on the MS-COCO [24] dataset, which comprises approximately 120K images in total, each accompanied by 5 captions. Due to the computational costs of high-resolution generation, we randomly sample 10K images from MS-COCO, assigning a fixed caption to each as input. To ensure

Methods	Image Quality	Semantics	Preference
SDM	2.60	2.05	5.42%
SDM-MegaFusion	3.25	4.40	12.92%
SDM-MegaFusion++	4.25	4.55	81.66%
Floyd-Stage2	2.18	4.28	1.67%
Floyd-MegaFusion	3.45	4.58	21.25%
Floyd-MegaFusion++	4.22	4.58	77.08%

Table 2. **Human evaluation** with MS-COCO captions and commonly used prompts from the Internet as input.

a consistent comparison, we utilize the same random seed for each image across different methods, neutralizing randomness. For qualitative human evaluations, we use commonly available prompts from the Internet as text conditions, and conditional images provided by the original code repositories as extra inputs for IP-Adapter and ControlNet.

Evaluation Metrics. To evaluate the quality of generated images, we adopt several widely-used metrics, including Fréchet Inception Distance score (FID) [13], Kernel Inception Distance score (KID), and CLIP [31] text-image similarity (CLIP-T). Following previous works [11], we consider two types of FID and KID: (i) FID_r and KID_r to gauge the quality and diversity of generated images relative to real ones, and (ii) FID_b and KID_b to assess the discrepancy between synthesized samples under the base training resolution and those at high resolution. These latter metrics reflect the model’s capability to retain generative proficiency at unfamiliar resolutions.

To evaluate the semantic accuracy of generated contents, we adopt MiniGPT-v2 [4] to caption the images, and calculate several linguistic metrics between these captions and the original input text. Concretely, we report the commonly used CIDEr [42], Meteor [1], and ROUGE [23]. Moreover, we detail the GFlops and inference time measured on a single A40 GPU for efficiency comparison.

5.2. Quantitative Results

Objective Metrics. We compare the performance of both latent-space and pixel-space diffusion models boosted by our **MegaFusion** with their baseline counterparts on the MS-COCO [24] dataset. Here, [model-MegaFusion] refers to models employing *truncate and relay* strategy to bridge multi-resolution generation, while [model-MegaFusion++] denotes advanced models that incorporate *dilated convolution* and *noise re-scheduling*. We also compare with several existing state-of-the-art methods, such as SDM with StableSR [44], ScaleCrafter [11], and DemoFusion [7], which are limited to specific latent-space models and less efficient.

The results in Table 1 highlight significant improvements with MegaFusion across all metrics, including image quality, semantic accuracy, and especially computational efficiency. This indicates that our MegaFusion effectively ex-

tends the generative capabilities of existing diffusion models towards synthesizing high-resolution images with correct semantics and details while using only about 40% of the computational cost. Furthermore, incorporating *dilated convolution* and *noise re-scheduling* further improves performance on metrics such as FID_r , KID_r , CLIP-T, and ROUGE, reflecting an improvement in generation diversity and alignment with real images and text conditions.

Human Assessment. To complement our objective analysis, we conduct a human-centric evaluation focusing on image quality and semantic integrity. Concretely, utilizing the same text and random seed as inputs, we synthesize higher-resolution images via standard models (SDM and Floyd) and their MegaFusion-boosted counterparts. Participants are asked to rate the outputs with a score from 1 to 5 (the higher, the better), considering both image quality and semantic accuracy. Moreover, they also need to select their favourite image among the options for preference rating.

The results in Table 2 affirm that our MegaFusion significantly improves the performance of higher-resolution image generation in terms of image quality and semantic accuracy. Additionally, our advanced MegaFusion++ demonstrates the potential for greater improvements. This evidence underscores MegaFusion’s ability to elevate pre-trained models, enabling them to produce higher-resolution images with superior quality and accurate semantics.

5.3. Qualitative Results

Comparison on text-to-image foundation models. Figure 3 showcases visualization results of higher-resolution image generation in both latent and pixel spaces. These results affirm that MegaFusion can be seamlessly integrated with existing diffusion models to produce images of megapixels with accurate semantics, whereas prior baselines fail to do so. Moreover, incorporating dilated convolutions and noise re-scheduling further improves image details. Additional results are available in the Appendix.

Comparison on models with additional conditions. We further apply MegaFusion to diffusion models equipped with extra input conditions, such as IP-Adapter and ControlNet, as illustrated in Figure 4. Our MegaFusion exhibits universal applicability, significantly extending the capacity of various diffusion models to synthesize high-quality images of higher resolutions, which not only adhere to the input conditions but also maintain semantic integrity.

5.4. Ablation Studies

Proposed strategy & modules. To evaluate the efficacy of our proposed strategy and components, we assess several model variants in both latent and pixel spaces. Here, ‘T&R’, ‘D’, and ‘R’ represent *truncate and relay* strategy, *dilated convolution*, and *noise re-scheduling*, respectively. The results in Table 3 demonstrate that our strategy and

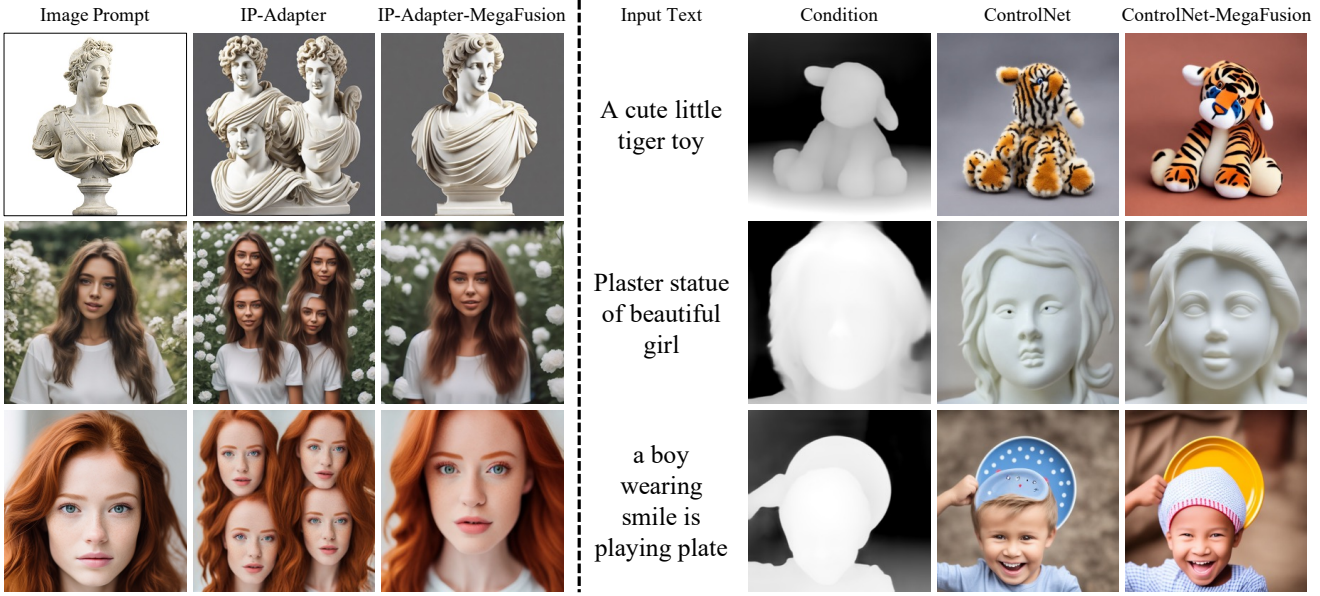


Figure 4. **Qualitative results** of incorporating our method to models with extra conditional inputs. Our proposed MegaFusion can be universally applied across various diffusion models, providing the capability for higher-resolution image generation with better semantics and fidelity. Please refer to the Appendix for more qualitative results.

Methods	T&R	D	R	FID _r	FID _b	KID _r	KID _b
SDM [35]	✗	✗	✗	41.35	51.02	0.0086	0.0113
SDM-MegaFusion	✓	✗	✗	30.19	10.98	0.0088	0.0034
SDM-MegaFusion-D	✓	✓	✗	27.56	9.34	0.0075	0.0019
SDM-MegaFusion-R	✓	✗	✓	26.78	9.34	0.0075	0.0019
SDM-MegaFusion++	✓	✓	✓	25.14	7.82	0.0064	0.0012
Floyd-Stage1	✗	✗	✗	66.27	81.65	0.0262	0.0454
Floyd-MegaFusion	✓	✗	✗	53.09	39.73	0.0273	0.0334
Floyd-MegaFusion-D	✓	✓	✗	51.76	41.96	0.0268	0.0345
Floyd-MegaFusion-R	✓	✗	✓	44.27	49.38	0.0215	0.0431
Floyd-MegaFusion++	✓	✓	✓	43.43	50.08	0.0213	0.0437

Table 3. **Ablation Study** on proposed modules in MegaFusion on MS-COCO [24]. The modules gradually improve the higher-resolution image generation quality of existing diffusion models, especially in comparison with real images.

modules substantially elevate the quality and diversity of contents generated by foundational generative models such as SDM (1024×1024) and Floyd (128×128), especially improving the quality and fidelity to real-world images.

Upsampler Φ . In our *truncate and relay* strategy, a non-parametric Upsampler plays a crucial role in bridging generation processes across different resolutions. To discern the optimal choice, we evaluate several configurations of the SDM-MegaFusion++ model on MS-COCO dataset. These variants include Config-A with bilinear upsampling; Config-B with bicubic upsampling; Config-C incorporating bicubic coupled with a 5×5 Gaussian filter, and Config-D employing bicubic alongside a 3×3 edge-enhancement

Methods	FID _r \downarrow	FID _b \downarrow	KID _r \downarrow	KID _b \downarrow
SDM	41.35	51.02	0.0086	0.0113
Config-A	28.03	9.70	0.0076	0.0020
Config-B	25.14	7.82	0.0064	0.0012
Config-C	35.07	18.10	0.0118	0.0063
Config-D	26.56	13.26	0.0065	0.0021

Table 4. **Ablation study** on non-parametric Upsampler function Φ on the MS-COCO dataset.

kernel. As depicted in Table 4, SDM-MegaFusion++ with Config-B emerges as the superior method in terms of both FID and KID metrics. Consequently, we have designated bicubic upsampling as the default choice.

6. Conclusion

In this paper, we introduce **MegaFusion**, a tuning-free approach designed to tackle the challenges of synthesizing higher-resolution images, which effectively addresses issues of semantic inaccuracies and object replication. Our method adopts an innovative *truncate and relay* strategy to elegantly connect generation processes across different resolutions, efficiently synthesizing high-quality higher-resolution images of megapixels and various aspect ratios in a coarse-to-fine manner. By incorporating orthogonal *dilated convolutions* and *noise re-scheduling*, we further adapt the model priors towards higher resolution. The versatility and efficacy of our MegaFusion enable it universally applicable to both latent-space and pixel-space diffusion models, as well as their extensions with extra condi-

tions. Extensive experiments have validated the superiority of MegaFusion, demonstrating its capability to generate images at higher resolutions with only about 40% of the original computational cost.

References

[1] Satanjeev Banerjee and Alon Lavie. Meteor: An automatic metric for mt evaluation with improved correlation with human judgments. In *Proceedings of the acl workshop on intrinsic and extrinsic evaluation measures for machine translation and/or summarization*, pages 65–72, 2005. 7

[2] Omer Bar-Tal, Lior Yariv, Yaron Lipman, and Tali Dekel. MultiDiffusion: Fusing diffusion paths for controlled image generation. In *Proceedings of the International Conference on Machine Learning*, pages 1737–1752. PMLR, 2023. 2

[3] Tim Brooks, Aleksander Holynski, and Alexei A. Efros. Instructpix2pix: Learning to follow image editing instructions. In *Proceedings of the IEEE Conference on Computer Vision and Pattern Recognition*, 2023. 1, 2

[4] Jun Chen, Deyao Zhu, Xiaoqian Shen, Xiang Li, Zechun Liu, Pengchuan Zhang, Raghuraman Krishnamoorthi, Vikas Chandra, Yunyang Xiong, and Mohamed Elhoseiny. Minigpt-v2: large language model as a unified interface for vision-language multi-task learning. *arXiv preprint arXiv:2310.09478*, 2023. 7

[5] Jiaxiang Cheng, Pan Xie, Xin Xia, Jiashi Li, Jie Wu, Yuxi Ren, Huixia Li, Xuefeng Xiao, Min Zheng, and Lean Fu. Resadapter: Domain consistent resolution adapter for diffusion models. *arXiv preprint arXiv:2403.02084*, 2024. 2, 3

[6] Deepfloyd. Deepfloyd. URL <https://www.deepfloyd.ai/>, 2023. 1, 2, 5, 6, 12, 13, 16

[7] Ruoyi Du, Dongliang Chang, Timothy Hospedales, Yi-Zhe Song, and Zhanyu Ma. Demofusion: Democratising high-resolution image generation with no \$++. In *Proceedings of the IEEE Conference on Computer Vision and Pattern Recognition*, 2024. 3, 5, 7, 12, 13, 17

[8] Ian Goodfellow, Jean Pouget-Abadie, Mehdi Mirza, Bing Xu, David Warde-Farley, Sherjil Ozair, Aaron Courville, and Yoshua Bengio. Generative adversarial networks. *Communications of the ACM*, 2020. 2

[9] Lanqing Guo, Yingqing He, Haoxin Chen, Menghan Xia, Xiaodong Cun, Yufei Wang, Siyu Huang, Yong Zhang, Xintao Wang, Qifeng Chen, et al. Make a cheap scaling: A self-cascade diffusion model for higher-resolution adaptation. *arXiv preprint arXiv:2402.10491*, 2024. 2, 3

[10] Moayed Haji-Ali, Guha Balakrishnan, and Vicente Ordonez. Elastcdiffusion: Training-free arbitrary size image generation. *arXiv preprint arXiv:2311.18822*, 2023. 2

[11] Yingqing He, Shaoshu Yang, Haoxin Chen, Xiaodong Cun, Menghan Xia, Yong Zhang, Xintao Wang, Ran He, Qifeng Chen, and Ying Shan. Scalecrafter: Tuning-free higher-resolution visual generation with diffusion models. In *Proceedings of the International Conference on Learning Representations*, 2023. 2, 3, 4, 5, 7, 13, 17

[12] Amir Hertz, Ron Mokady, Jay Tenenbaum, Kfir Aberman, Yael Pritch, and Daniel Cohen-Or. Prompt-to-prompt image editing with cross attention control. In *Proceedings of the International Conference on Learning Representations*, 2023. 1, 2

[13] Martin Heusel, Hubert Ramsauer, Thomas Unterthiner, Bernhard Nessler, and Sepp Hochreiter. Gans trained by a two time-scale update rule converge to a local nash equilibrium. In *Advances in Neural Information Processing Systems*, 2017. 7

[14] Jonathan Ho, William Chan, Chitwan Saharia, Jay Whang, Ruiqi Gao, Alexey Gritsenko, Diederik P Kingma, Ben Poole, Mohammad Norouzi, David J Fleet, et al. Imagen video: High definition video generation with diffusion models. *arXiv preprint arXiv:2210.02303*, 2022. 1, 2

[15] Jonathan Ho, Ajay Jain, and Pieter Abbeel. Denoising diffusion probabilistic models. In *Advances in Neural Information Processing Systems*, 2020. 1, 2

[16] Jonathan Ho and Tim Salimans. Classifier-free diffusion guidance. In *NeurIPS 2021 Workshop on Deep Generative Models and Downstream Applications*, 2021. 1

[17] Jonathan Ho, Tim Salimans, Alexey Gritsenko, William Chan, Mohammad Norouzi, and David J Fleet. Video diffusion models. In *Advances in Neural Information Processing Systems*, 2022. 2

[18] Emiel Hoogeboom, Jonathan Heek, and Tim Salimans. Simple diffusion: End-to-end diffusion for high resolution images, 2023. 5, 12

[19] Edward J Hu, Yelong Shen, Phillip Wallis, Zeyuan Allen-Zhu, Yuanzhi Li, Shean Wang, Lu Wang, and Weizhu Chen. Lora: Low-rank adaptation of large language models. In *Proceedings of the International Conference on Learning Representations*, 2022. 2

[20] Linjiang Huang, Rongyao Fang, Aiping Zhang, Guanglu Song, Si Liu, Yu Liu, and Hongsheng Li. Fouriscale: A frequency perspective on training-free high-resolution image synthesis. *arXiv preprint arXiv:2403.12963*, 2024. 2, 3

[21] Bahjat Kawar, Shiran Zada, Oran Lang, Omer Tov, Huiwen Chang, Tali Dekel, Inbar Mosseri, and Michal Irani. Imagic: Text-based real image editing with diffusion models. In *Proceedings of the IEEE Conference on Computer Vision and Pattern Recognition*, 2023. 1, 2

[22] Diederik P Kingma and Max Welling. Auto-encoding variational bayes. In *Proceedings of the International Conference on Learning Representations*, 2014. 2

[23] Chin-Yew Lin. Rouge: A package for automatic evaluation of summaries. In *Text summarization branches out*, pages 74–81, 2004. 7

[24] Tsung-Yi Lin, Michael Maire, Serge Belongie, James Hays, Pietro Perona, Deva Ramanan, Piotr Dollár, and C Lawrence Zitnick. Microsoft coco: Common objects in context. In *Proceedings of the European Conference on Computer Vision*, 2014. 5, 6, 7, 8, 12, 15, 16

[25] Chang Liu, Haoning Wu, Yujie Zhong, Xiaoyun Zhang, Yanfeng Wang, and Weidi Xie. Intelligent grimm – open-ended visual storytelling via latent diffusion models. In *Proceedings of the IEEE Conference on Computer Vision and Pattern Recognition*, 2024. 1, 2

[26] Andreas Lugmayr, Martin Danelljan, Andres Romero, Fisher Yu, Radu Timofte, and Luc Van Gool. Repaint: Inpainting

using denoising diffusion probabilistic models. In *Proceedings of the IEEE Conference on Computer Vision and Pattern Recognition*, 2022. 1, 2

[27] Adyasha Maharana, Darryl Hannan, and Mohit Bansal. Storydall-e: Adapting pretrained text-to-image transformers for story continuation. In *Proceedings of the European Conference on Computer Vision*, 2022. 1, 2

[28] Chenlin Meng, Yutong He, Yang Song, Jiaming Song, Jiajun Wu, Jun-Yan Zhu, and Stefano Ermon. Sdedit: Guided image synthesis and editing with stochastic differential equations. In *Proceedings of the International Conference on Learning Representations*, 2021. 1, 2

[29] Xichen Pan, Pengda Qin, Yuhong Li, Hui Xue, and Wenhui Chen. Synthesizing coherent story with auto-regressive latent diffusion models. In *Winter Conference on Applications of Computer Vision*, 2024. 1, 2

[30] Dustin Podell, Zion English, Kyle Lacey, Andreas Blattmann, Tim Dockhorn, Jonas Müller, Joe Penna, and Robin Rombach. Sdxl: Improving latent diffusion models for high-resolution image synthesis. *arXiv preprint arXiv:2307.01952*, 2023. 1, 2, 5, 6, 13, 14, 19, 20, 21

[31] Alec Radford, Jong Wook Kim, Chris Hallacy, Aditya Ramesh, Gabriel Goh, Sandhini Agarwal, Girish Sastry, Amanda Askell, Pamela Mishkin, Jack Clark, et al. Learning transferable visual models from natural language supervision. In *Proceedings of the International Conference on Machine Learning*, 2021. 3, 7

[32] Colin Raffel, Noam Shazeer, Adam Roberts, Katherine Lee, Sharan Narang, Michael Matena, Yanqi Zhou, Wei Li, and Peter J Liu. Exploring the limits of transfer learning with a unified text-to-text transformer. *The Journal of Machine Learning Research*, 2020. 3

[33] Aditya Ramesh, Prafulla Dhariwal, Alex Nichol, Casey Chu, and Mark Chen. Hierarchical text-conditional image generation with clip latents. *arXiv preprint arXiv:2204.06125*, 2022. 2

[34] Aditya Ramesh, Mikhail Pavlov, Gabriel Goh, Scott Gray, Chelsea Voss, Alec Radford, Mark Chen, and Ilya Sutskever. Zero-shot text-to-image generation. In *Proceedings of the International Conference on Machine Learning*, 2021. 2

[35] Robin Rombach, Andreas Blattmann, Dominik Lorenz, Patrick Esser, and Bjorn Ommer. High-resolution image synthesis with latent diffusion models. In *Proceedings of the IEEE Conference on Computer Vision and Pattern Recognition*, 2022. 1, 2, 5, 6, 8, 13, 15

[36] Olaf Ronneberger, Philipp Fischer, and Thomas Brox. U-net: Convolutional networks for biomedical image segmentation. In *Medical Image Computing and Computer-Assisted Intervention–MICCAI 2015: 18th International Conference, Munich, Germany, October 5–9, 2015, Proceedings, Part III* 18, 2015. 3

[37] Chitwan Saharia, William Chan, Saurabh Saxena, Lala Li, Jay Whang, Emily L Denton, Kamyar Ghasemipour, Raphael Gontijo Lopes, Burcu Karagol Ayan, Tim Salimans, et al. Photorealistic text-to-image diffusion models with deep language understanding. In *Advances in Neural Information Processing Systems*, 2022. 2

[38] Christoph Schuhmann, Romain Beaumont, Richard Vencu, Cade W Gordon, Ross Wightman, Mehdi Cherti, Theo Coombes, Aarush Katta, Clayton Mullis, Mitchell Wortsman, Patrick Schramowski, Srivatsa R Kundurthy, Katherine Crowson, Ludwig Schmidt, Robert Kaczmarczyk, and Jenia Jitsev. LAION-5b: An open large-scale dataset for training next generation image-text models. In *Advances in Neural Information Processing Systems*, 2022. 2

[39] Uriel Singer, Adam Polyak, Thomas Hayes, Xi Yin, Jie An, Songyang Zhang, Qiyuan Hu, Harry Yang, Oron Ashual, Oran Gafni, et al. Make-a-video: Text-to-video generation without text-video data. In *Proceedings of the International Conference on Learning Representations*, 2023. 2

[40] Jiaming Song, Chenlin Meng, and Stefano Ermon. Denoising diffusion implicit models. In *Proceedings of the International Conference on Learning Representations*, 2020. 1, 2, 6

[41] Jiayan Teng, Wendi Zheng, Ming Ding, Wenyi Hong, Jianqiao Wangni, Zhuoyi Yang, and Jie Tang. Relay diffusion: Unifying diffusion process across resolutions for image synthesis. In *Proceedings of the International Conference on Learning Representations*, 2024. 2, 5

[42] Ramakrishna Vedantam, C Lawrence Zitnick, and Devi Parikh. Cider: Consensus-based image description evaluation. In *Proceedings of the IEEE Conference on Computer Vision and Pattern Recognition*, pages 4566–4575, 2015. 7

[43] Catherine Wah, Steve Branson, Peter Welinder, Pietro Perona, and Serge J. Belongie. The caltech-ucsd birds-200-2011 dataset. 2011. 12, 13

[44] Jianyi Wang, Zongsheng Yue, Shangchen Zhou, Kelvin CK Chan, and Chen Change Loy. Exploiting diffusion prior for real-world image super-resolution. In *arXiv preprint arXiv:2305.07015*, 2023. 5, 7

[45] Shaoan Xie, Zhifei Zhang, Zhe Lin, Tobias Hinz, and Kun Zhang. Smartbrush: Text and shape guided object inpainting with diffusion model. In *Proceedings of the IEEE Conference on Computer Vision and Pattern Recognition*, 2023. 1, 2

[46] Li Xin, Chu Wenqing, Wu Ye, Yuan Weihang, Liu Fanglong, Zhang Qi, Li Fu, Feng Haocheng, Ding Errui, and Wang Jingdong. Videogen: A reference-guided latent diffusion approach for high definition text-to-video generation. *arXiv preprint arXiv:2309.00398*, 2023. 2

[47] Tao Xu, Pengchuan Zhang, Qiuyuan Huang, Han Zhang, Zhe Gan, Xiaolei Huang, and Xiaodong He. Attngan: Fine-grained text to image generation with attentional generative adversarial networks. In *Proceedings of the IEEE Conference on Computer Vision and Pattern Recognition*, 2018. 2

[48] Hu Ye, Jun Zhang, Sibo Liu, Xiao Han, and Wei Yang. Ipadapter: Text compatible image prompt adapter for text-to-image diffusion models. *arXiv preprint arXiv:2308.06721*, 2023. 2, 5, 14

[49] Fisher Yu and Vladlen Koltun. Multi-scale context aggregation by dilated convolutions, 2016. 2, 4

[50] Han Zhang, Tao Xu, Hongsheng Li, Shaoting Zhang, Xiaogang Wang, Xiaolei Huang, and Dimitris N Metaxas. Stackgan: Text to photo-realistic image synthesis with stacked

generative adversarial networks. In *Proceedings of the International Conference on Computer Vision*, 2017. 2

[51] Lvmin Zhang, Anyi Rao, and Maneesh Agrawala. Adding conditional control to text-to-image diffusion models. In *Proceedings of the International Conference on Computer Vision*, 2023. 2, 5, 14, 18

[52] Shen Zhang, Zhaowei Chen, Zhenyu Zhao, Yuhao Chen, Yao Tang, and Jiajun Liang. Hidiffusion: Unlocking higher-resolution creativity and efficiency in pretrained diffusion models. *arXiv preprint arXiv:2311.17528*, 2023. 3

In this appendix, we start by giving more details on the implementation details of our proposed MegaFusion in Section A. Then, we provide extra quantitative comparisons to further demonstrate the universality and effectiveness of our method in Section B. Next, we offer additional qualitative results across various experimental settings and methods to illustrate the superiority of our proposed MegaFusion in Section C. Finally, we discuss the limitations of our method and future work in Section D.

A. Implementation Details

More Details on Floyd-MegaFusion. We have evaluated the higher-resolution image generation performance of the Floyd [6] model at resolutions of 128×128 and 512×512 . For 128×128 resolution, we directly apply MegaFusion to the first stage of the Floyd model. As for the comparison at 512×512 resolution, we utilize the first two stages of the Floyd model. Considering that the quality of the results from the first stage generation would significantly affect the second generation stage, we opt for using the 64×64 images generated by the original first stage model as inputs of both the baseline and our boosted Floyd-MegaFusion. That is, higher-resolution image generation is only performed under the second generation stage. Ultimately, the experimental results presented in Table 1 effectively demonstrate the universality and effectiveness of our proposed MegaFusion. Furthermore, we also conduct experiments where 128×128 out-of-distribution images are generated in the first stage, followed by 512×512 resolution images in the second stage. This further demonstrates that MegaFusion maintains semantic accuracy across all stages of generation.

Details on Human Evaluation. To more effectively reflect the performance of different models in generating high-resolution images, we have recruited 10 volunteers with a background in image generation research for human evaluation. Specifically, the evaluators are asked to follow these rules: (i) Rate unknown source images on a score from 1 to 5 for both image quality and semantic accuracy, with higher scores indicating better quality; and (ii) Observe the results generated by different models with the same input conditions and select their favourite one based on a comprehensive consideration of quality and semantics.

B. Additional Quantitative Results

B.1. Comparison on crop FID/KID

Following previous work [7], we also calculate the crop FID and crop KID metrics on the generated results of various models to reflect the quality of local patches in the generated images. As depicted in Table 5, previous methods are often limited to specific latent-space models, while our MegaFusion consistently improves the quality of high-

resolution image generation in both latent-space and pixel-space models.

Method	SDM-1024	SDXL-2048	Floyd-128	Floyd-512
Original	41.21/0.0139	42.29/0.0125	70.16/0.0224	40.65/0.0171
ScaleCrafter	32.24 /0.0085	26.58/0.0062	inapplicable	inapplicable
DemoFusion	inapplicable	25.91/0.0061	inapplicable	inapplicable
MegaFusion	39.42/0.0137	27.38/0.0063	57.24/0.0243	32.36/0.0122
MegaFusion++	33.39/ 0.0084	25.64 / 0.0049	41.22 / 0.0188	29.18 / 0.0077

Table 5. Comparison of $\text{FID}_{\text{crop}}/\text{KID}_{\text{crop}}$ on MS-COCO dataset.

B.2. Comparison on CUB-200 Dataset

To demonstrate the universality of our proposed MegaFusion, in addition to the MS-COCO [24] dataset, we also conduct quantitative evaluations on the CUB-200 [43] dataset, which is also commonly used in previous works. The CUB-200 dataset consists of over 10K images of 200 categories of birds, each accompanied by 10 textual descriptions. Considering computational costs and time expenditure, similar to the experimental settings on the MS-COCO dataset in our manuscript, we randomly select 1K images from the CUB-200 dataset. Each image is assigned a fixed caption, and the same random seed is used across different methods to eliminate the effects of randomness among models. As depicted in Table 6, our proposed MegaFusion can also be universally applied to both latent-space and pixel-space diffusion models on the CUB-200 dataset, achieving high-quality higher-resolution image generation.

B.3. More Results of Floyd-MegaFusion

As mentioned above, we also conduct experiments that first generate 128×128 out-of-distribution images, followed by 512×512 high-resolution images on the Floyd model. As depicted in Table 7, under both settings, MegaFusion effectively improves the high-resolution generation capability of Floyd. This demonstrates that MegaFusion can improve the semantic accuracy of high-resolution images at any stage of the generation process.

C. Additional Qualitative Results

C.1. Effects of hyperparameters δ and γ

For denoising at the original size, we do not employ dilation. During qualitative experiments for high-resolution generation, we test different δ values and find that $\delta = 2$ is a stable choice for our method and experiment settings, which will not introduce blurriness or semantic deviations. As described in our manuscript, we draw inspiration from simple diffusion [18], which derives the SNR relationship between different resolution images from the mean and variance of pixel distributions. Substituting this into our derived relationship, we obtain that $\gamma = 4$. Qualitative experiments

Methods	resolution	$\text{FID}_r \downarrow$	$\text{FID}_b \downarrow$	$\text{KID}_r \downarrow$	$\text{KID}_b \downarrow$	$\text{CLIP-T} \uparrow$	$\text{CIDEr} \uparrow$	$\text{Meteor} \uparrow$	$\text{ROUGE} \uparrow$	GFlops	Inference time
SDM [35]	1024×1024	77.92	46.34	0.0363	0.0220	0.2952	8.12	7.48	7.09	135.0K	15.17s
SDM-MegaFusion	1024×1024	71.78	36.21	0.0303	0.0189	0.3060	24.46	11.98	12.62	48.2K	7.56s
SDM-MegaFusion++	1024×1024	68.92	34.94	0.0251	0.0182	0.3115	28.52	12.32	13.29	48.2K	7.56s
SDXL [30]	2048×2048	73.49	48.78	0.0308	0.0274	0.2994	16.43	9.90	10.35	540.2K	79.66s
SDXL-MegaFusion	2048×2048	72.62	13.72	0.0296	0.0039	0.3113	25.98	13.23	13.33	216.1K	30.94s
SDXL-MegaFusion++	2048×2048	65.10	11.55	0.0225	0.0026	0.3122	26.35	13.98	14.92	216.1K	30.94s
Floyd-Stage1 [6]	128×128	87.04	105.59	0.0341	0.0658	0.2866	9.95	8.28	9.07	111.7K	77.08s
Floyd-MegaFusion	128×128	77.82	36.49	0.0413	0.0281	0.3080	22.12	17.06	20.62	44.9K	32.19s
Floyd-MegaFusion++	128×128	73.54	45.76	0.0334	0.0388	0.3086	22.52	16.93	20.05	44.9K	32.19s
Floyd-Stage2 [6]	512×512	80.34	41.65	0.0401	0.0215	0.3013	23.59	12.28	11.67	60.7K	48.58s
Floyd-MegaFusion	512×512	77.66	39.34	0.0348	0.0141	0.3110	24.63	15.74	15.29	24.3K	21.72s
Floyd-MegaFusion++	512×512	62.91	34.40	0.0232	0.0115	0.3141	25.44	13.90	18.51	24.3K	21.72s

Table 6. **Quantitative comparison** on CUB-200 [43] dataset. **RED**: best performance, **BLUE**: second best performance.

Methods	resolution	$\text{FID}_r \downarrow$	$\text{FID}_b \downarrow$	$\text{KID}_r \downarrow$	$\text{KID}_b \downarrow$	$\text{CLIP-T} \uparrow$	$\text{CIDEr} \uparrow$	$\text{Meteor} \uparrow$	$\text{ROUGE} \uparrow$	GFlops	Inference time
Floyd-Stage1 [6]	128×128	66.27	81.65	0.0262	0.0454	0.2818	14.69	18.22	25.06	111.7K	77.08s
Floyd-MegaFusion	128×128	53.09	39.73	0.0273	0.0334	0.3024	25.01	25.00	31.35	44.9K	32.19s
Floyd-MegaFusion++	128×128	43.43	50.08	0.0213	0.0437	0.3046	20.28	25.01	31.64	44.9K	32.19s
Floyd-Stage2 [6]	$64 \rightarrow 512$	46.64	38.15	0.0254	0.0166	0.3098	23.85	21.47	26.26	60.7K	48.58s
Floyd-MegaFusion	$64 \rightarrow 512$	39.80	24.87	0.0164	0.0078	0.3106	23.22	23.51	29.30	24.3K	21.72s
Floyd-MegaFusion++	$64 \rightarrow 512$	26.34	24.55	0.0063	0.0077	0.3110	24.01	23.58	29.52	24.3K	21.72s
Floyd-Stage2 [6]	$128 \rightarrow 512$	61.24	108.01	0.0253	0.0734	0.2779	15.16	14.76	19.75	60.7K	48.58s
Floyd-MegaFusion	$128 \rightarrow 512$	58.19	88.56	0.0187	0.0379	0.2821	16.28	15.65	20.02	24.3K	21.72s
Floyd-MegaFusion++	$128 \rightarrow 512$	57.92	94.93	0.0181	0.0417	0.2835	16.36	15.47	21.34	24.3K	21.72s

Table 7. **More comparison results** on Floyd model and its MegaFusion boosted counterparts under different settings. Within each unit, we denote the best performance in **RED** and the second-best performance in **BLUE**.

also confirm that this is an appropriate choice. Some visualization examples are shown in Figure 5.

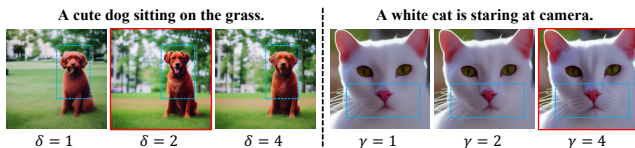


Figure 5. **Qualitative comparisons** of applying different hyper-parameters δ and γ .

C.2. Text-to-Image Foundation Models

We present more visualization results of higher-resolution image generation using both latent-space and pixel-space text-to-image models in Figure 6 and 7, respectively, to demonstrate the universality and robustness of our proposed method. The visual outcomes explicitly confirm that when pre-trained models fail to scale to higher resolutions, our approach can be universally integrated into existing latent-space and pixel-space diffusion models, improving their capability to synthesize higher-resolution images

of megapixels with accurate semantics. Moreover, our further enhanced MegaFusion++ significantly boosts the quality of the generated images, producing sharper and clearer details.

C.3. Comparison to state-of-the-art

To further demonstrate the quality of MegaFusion, we also compare it with existing state-of-the-art high-resolution generation methods. Given that these methods (ScaleCrafter [11] and DemoFusion [7]) are typically limited to specific models, we conduct comparisons on models based on SDXL. The results in Figure 8 indicate that existing methods still face quality degradation and object repetition when generating high-resolution images. In contrast, MegaFusion produces high-quality, semantically accurate high-resolution images. Additionally, as shown in Table 1, MegaFusion is much more efficient than existing approaches.

C.4. Models with additional conditions

We have confirmed that our method is equally applicable to diffusion models with additional input conditions, such as ControlNet [51] with depth maps and IP-Adapter [48] with reference images as extra inputs. As depicted in Figure 9, we further discover that ControlNet [51] with canny edges or human poses as additional conditional inputs also struggle with synthesizing higher-resolution images, and often produce images that are not fidelity to input conditions, with confusing semantics and poor image quality. In contrast, with the assistance of our proposed MegaFusion, our boosted model, ControlNet-MegaFusion is still capable of generating high-quality images of higher resolutions with correct semantics, that are fidelity to conditions. This further illustrates the limitations of existing pre-trained generative models and powerfully demonstrates the effectiveness and universality of our proposed strategy.

C.5. Generation with Arbitrary Aspect Ratios

As previously stated, our MegaFusion can also assist existing pre-trained diffusion models in generating images at arbitrary aspect ratios. As illustrated in Figure 10, 11 and 12, building upon the SDXL [30] model, we offer more qualitative results from SDXL-MegaFusion across various aspect ratios and resolutions, including $1:1$ (2048×2048), $16:9$ (1920×1080), $3:4$ (1536×2048), and $4:3$ (2048×1536). These impressive visual outcomes further demonstrate the scalability and superiority of our approach.

D. Limitations & Future Work

D.1. Limitations

Since our proposed MegaFusion is a tuning-free approach based on existing latent-space and pixel-space image generation models, it inevitably inherits some of the limitations of current diffusion-based generative models. For example, when with complex textual conditions as inputs, the generated content often struggles to accurately reflect the input prompts, particularly in aspects such as attribute binding and positional control. This may lead to a degradation in synthesis quality during high-resolution generation with MegaFusion. However, better and more powerful backbone models are expected to mitigate this issue, and when combined with MegaFusion, they are likely to produce higher-quality images at higher resolutions with low computational costs.

D.2. Future Work

The striking quantitative results produced by our proposed MegaFusion have confirmed its potential to address the limitations of existing diffusion-based generative models and to improve their capabilities to synthesize high-resolution outcomes. Additionally, we have also observed

that existing video generation models encounter significant semantic deviations and quality decline when generating contents that exceed their pre-trained spatial resolution and temporal length. Therefore, we anticipate further applying MegaFusion to current video generation models towards efficient and low-cost higher-resolution longer video content generation. Similarly, MegaFusion also holds the potential for extension to 3D object generation models and models for image and video editing, which are also left for future research.

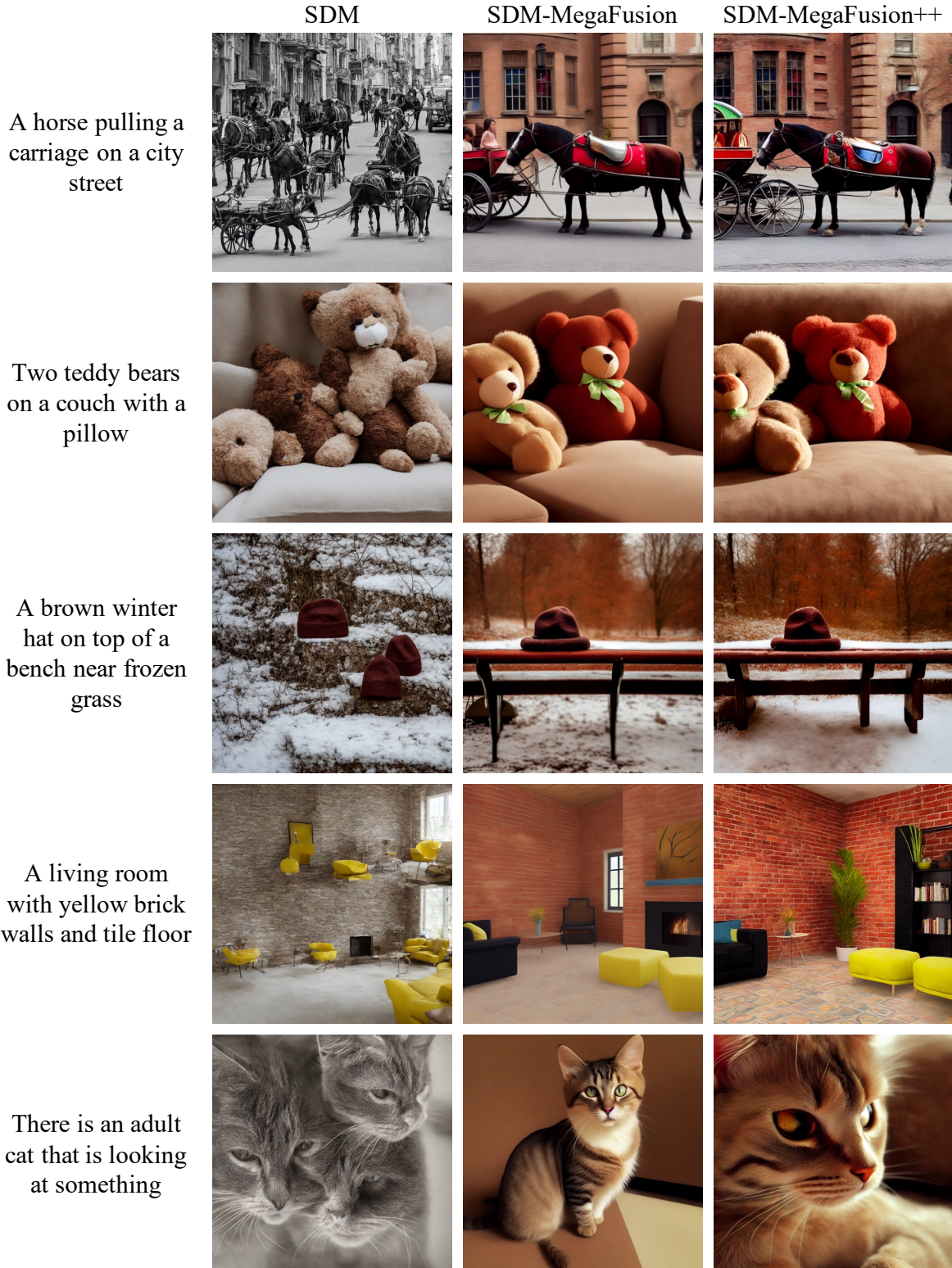


Figure 6. **More qualitative results** of applying our MegaFusion to latent-space diffusion model (SDM [35]) for higher-resolution image generation on MS-COCO [24] and commonly used prompts from the Internet.

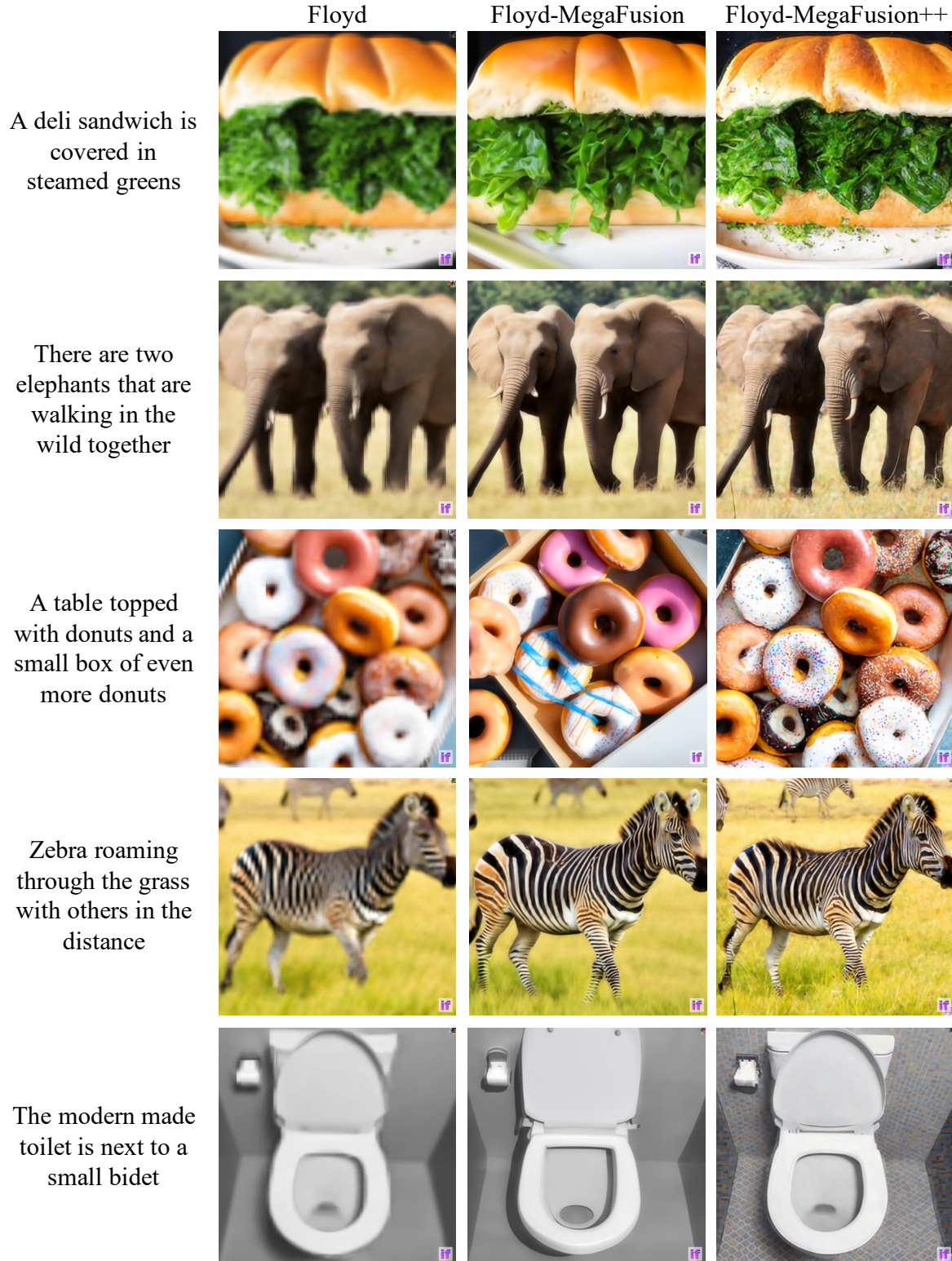


Figure 7. **More qualitative results** of applying our MegaFusion to pixel-space diffusion model (Floyd [6]) for higher-resolution image generation on MS-COCO [24] and commonly used prompts from the Internet.

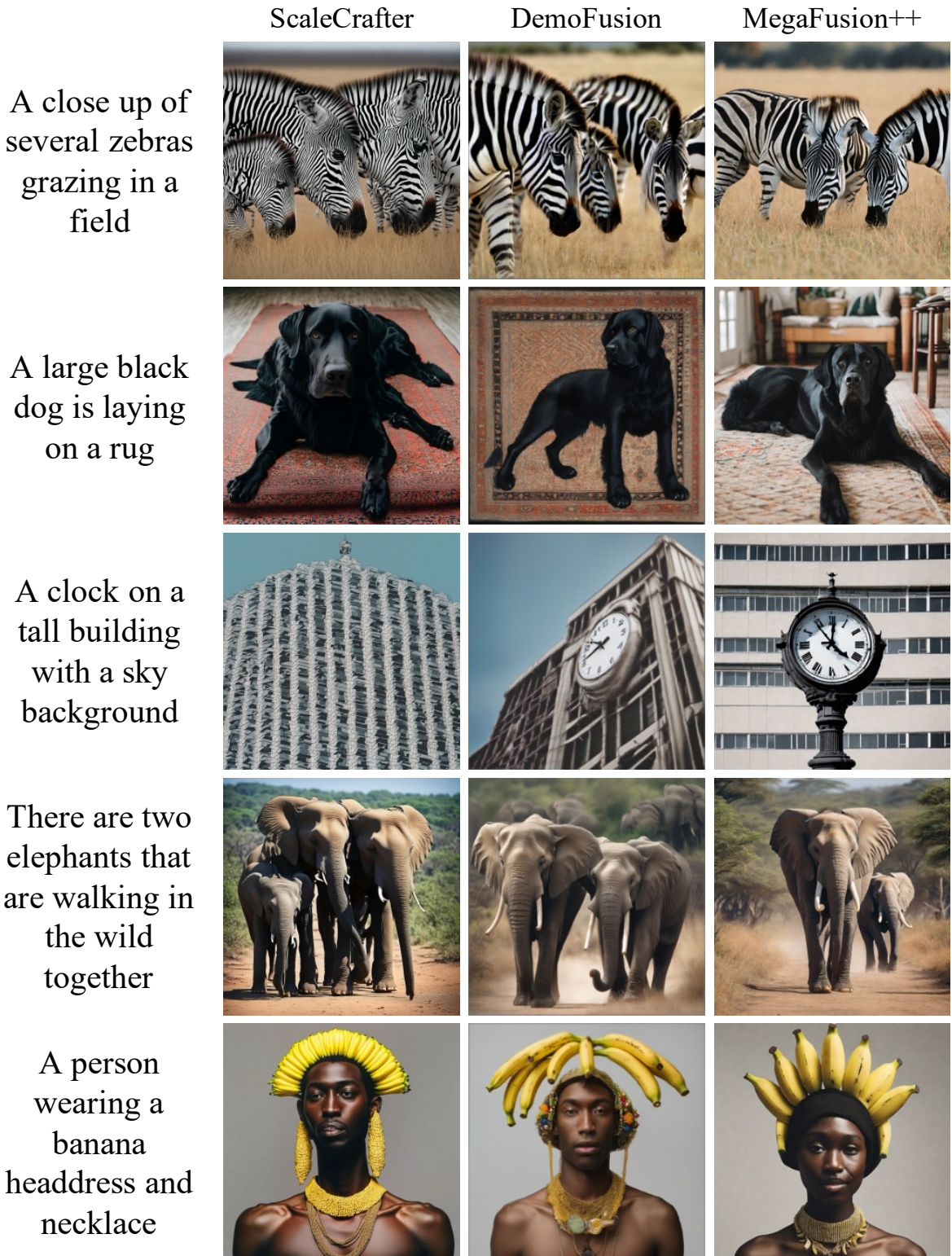


Figure 8. **Qualitative comparison** with existing state-of-the-art methods (ScaleCrafter [11] and DemoFusion [7]). Our MegaFusion can generate images with details and accurate semantics at high resolution, whereas existing methods struggle to do so.

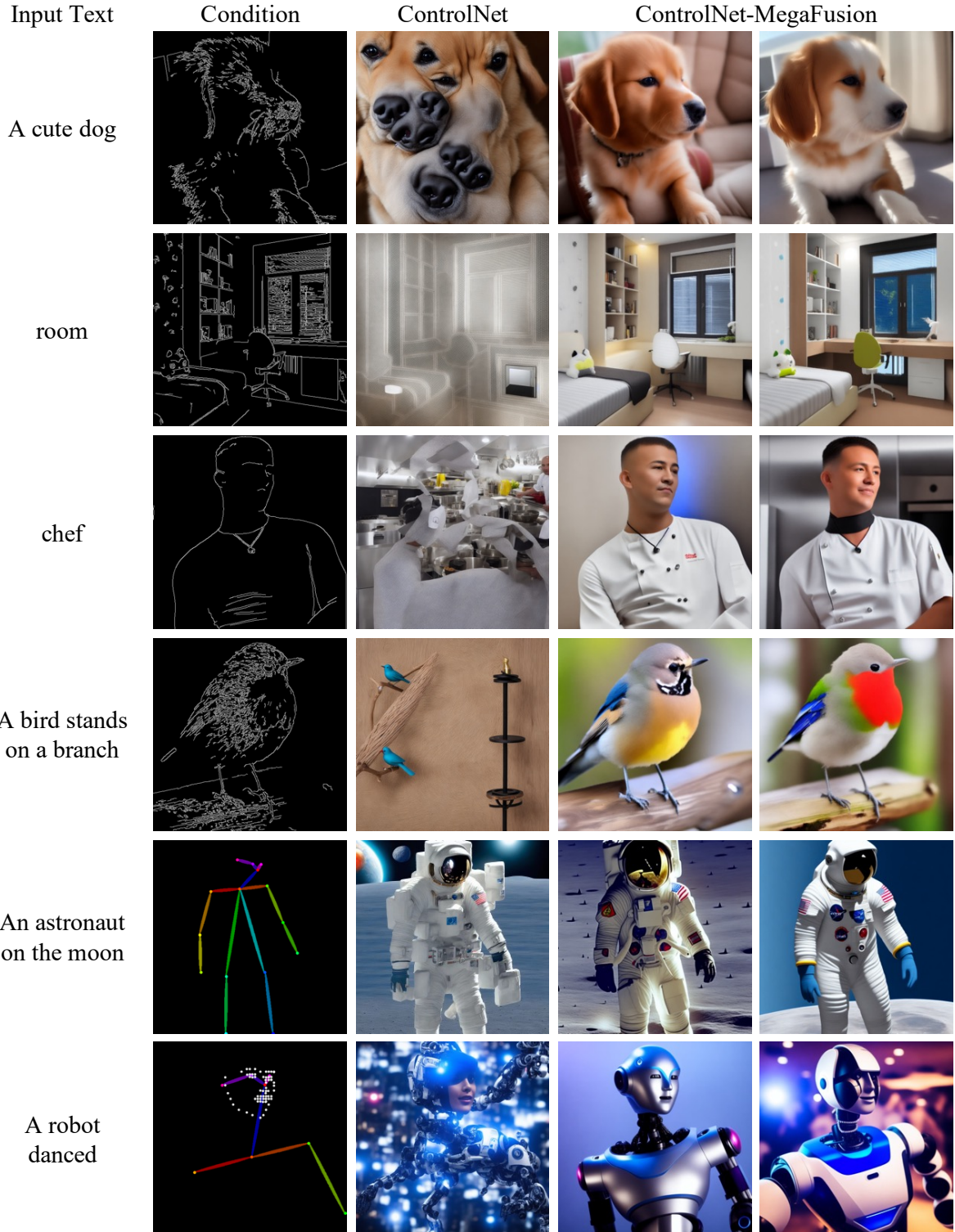


Figure 9. **Qualitative results** of applying our MegaFusion to ControlNet [51] with canny edges or human poses as extra conditions for higher-resolution image generation with better semantics and fidelity.



Figure 10. **More qualitative results** of applying our MegaFusion to SDXL [30] model for higher-resolution image generation with various aspect ratios and resolutions.



Figure 11. **More qualitative results** of applying our MegaFusion to SDXL [30] model for higher-resolution image generation with various aspect ratios and resolutions.

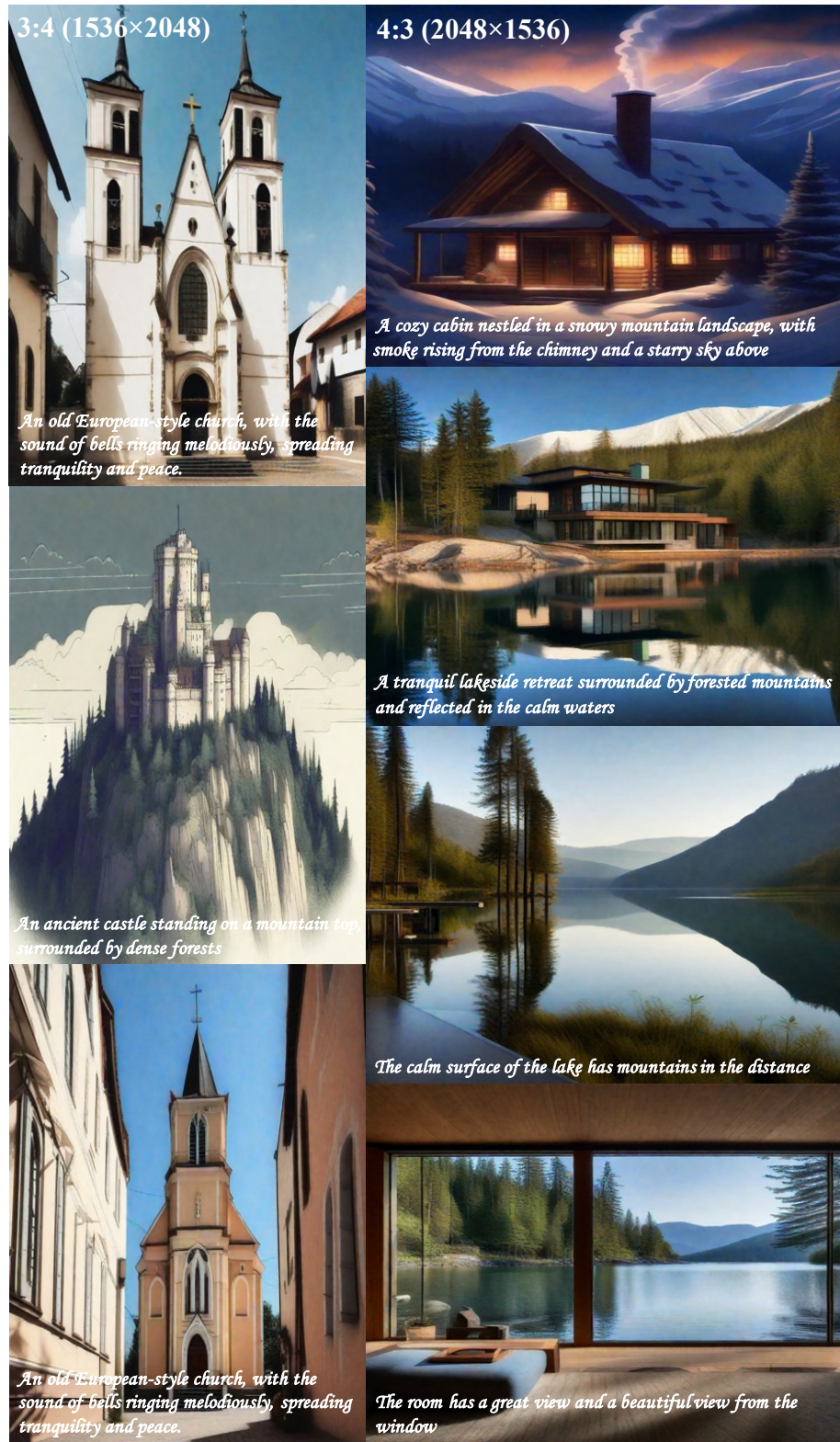


Figure 12. **More qualitative results** of applying our MegaFusion to SDXL [30] model for higher-resolution image generation with various aspect ratios and resolutions.